25th European Young Geotechnical Engineers Conference
21st – 24th of June 2016, Sibiu, Romania

Numerical analysis of penetration problems in clay with the Particle Finite Element Method

Lluís MONFORTE [1*]

[1] *Universitat Politècnica de Catalunya - BarcelonaTech, Departament d'Enginyeria del Terreny, Barcelona, SPAIN*

ABSTRACT

This paper highlights a computational framework for the numerical analysis of fluid saturated soil-structure interaction problems. The Particle Finite Element method is used to solve the linear momentum and mass of the mixture balance equations at large strains. The robustness and accuracy of the proposal is numerically demonstrated by means of the analysis of benchmark examples. Indeed, in the oedomeneter test example, it is shown that using a large deformation theory may reflect results that are artificially excluded by the linear theory. The paper concludes with a parametric analysis of a cone penetration test, where the influence of the contact roughness and permeability to the shaft friction and cone resistance are assessed.

Keywords: CPT, porous media, large strain, penetration test, PFEM.

1. INTRODUCTION

The Cone Penetration Test (CPT) is one of the most widely used in situ methods to characterize soil properties. The test method consists of pushing an instrumented cone into the ground at a controlled rate. During the penetration, measurements of the tip resistance and the friction at the sleeve are recorded. In addition, the pore water pressure may be measured at different locations.

Based on these measurements, constitutive soil parameters may be estimated with correlations. A large number of interpretation approaches have been obtained using a multitude of techniques, ranging from bearing capacity analogies to large deformation finite element simulations; however, there is still a large spread between the various proposals.

A large amount of numerical and analytical work has been devoted to the analysis of Cone Penetration test in undrained clay using a total stress approach. More recently, hydro-mechanical numerical analyses have been performed; the effect of partially drained conditions in the cone resistance and cone penetration consolidation test has been evaluated (Yi et al, 2012, Sheng et al, 2014).

The majority of hydromechanical numerical proposals only consider smooth interfaces between the soil and the structure. This hypothesis may be

* presenting author

unrealistic: as pointed out by Tsubakihara & Kishida (1993), that presented results of interface direct shear tests between clay and steel, the friction angle of the interface may be high: the clay friction angle was estimated at 27º whereas the angle of the interface was 23º.

Using a realistic description of soil behaviour (e.g. elasto-plastic effective stress response) increases both the range of conditions for and the precision of the interpretation. The downside is that a number of material non-linearities are added to a problem that already features severe geometric non-linearity.

Finite element method is well suited to include all sorts of non-linearities. However, when a Lagrangian formulation is employed –typically when a path dependent material model is used- the mesh may experience severe distortion, leading to numerical inaccuracies and even rendering the calculation impossible. In order to alleviate this problem several numerical techniques based on FEM have been proposed: adaptive methods, Arbitrary Lagrangian-Eulerian Material Point Method, among others.

In this work, the Particle Finite Element Method is employed to simulate the penetration of a rigid probe into the soil. The method is characterized by a particle discretization of the domain: every time-step a finite element mesh –whose nodes are the particles- is build using a Delaunay's tessellation and the solution is evaluated using a well shaped, low order finite element mesh (Oñate et al, 2004).

The soil-water mixture is modelled as a two-phase continuum employing a finite deformation formulation: the balance of linear momentum and mass of the mixture are written following the movement of the solid skeleton. The water flow is assumed to obey a generalization of the Darcy's Law whereas a multiplicative hyperelastic-plastic constitutive response is assumed for the solid skeleton.

The proposed approach is assessed against numerical benchmark examples. Finally, preliminary results of a parametric analysis of the Cone Penetration test are presented: the effect of the permeability and the friction angle of the cone-soil interface are evaluated.

2. NUMERICAL MODEL

This section outlines the numerical procedures used in this work. First the Particle Finite Element method (PFEM) is briefly reviewed; then, the balance equations are highlighted. Finally, the constitutive equations are described.

2.1. Particle Finite Element method

In the PFEM the continuum is modelled using an Updated Lagrangian formulation; that is, a Lagrangian description of the motion is used and all variables and their derivatives are referred to the deformed configuration. The nodes discretizing the analysis domain are treated as material particles whose motion is tracked during the transient solution; the interaction of these particles is computed using the finite element method and the particles serves as nodes of the FE mesh. Another particularity of PFEM is that only low order elements are used –linear triangles in 2D.

Periodically, the FE mesh is re-triangulated in order to alleviate problems that arise when the mesh becomes highly distorted. In addition, *h*-adaptive techniques are employed to obtain a better discretization in areas of the domain with large plastic deformations.

A typical solution algorithm involves the following steps (Oñate et al, 2004):

a. Discretize the domain with a Finite Element mesh. Define the shape and movement of the rigid structure.
b. Identify the external boundaries. Search the nodes that are in contact with the rigid structure.
c. Compute some time-steps of the coupled hydro-mechanical problem.
d. Construct a new mesh. This step may include a re-triangulation of the domain, introduce new particles in an adaptive fashion and interpolate

the state variables between the previous mesh and the new one.

e. Go back to step b. and repeat the solution process for the next time-steps.

2.2. Balance equations

The soil-water mixture is modelled as a two-phase continuum employing a finite deformation formulation. The equations of balance of linear momentum and mass of the mixture are written following the movement of the solid skeleton, where the unknown fields are the solid skeleton displacements and the fluid pressure (u-p_w formulation).

Excluding inertial effects, the Updated Lagrangian form of the governing equations read:

$$\begin{cases} \nabla \cdot \boldsymbol{\sigma} + \boldsymbol{b} = 0 & \text{in } \Omega_t \\ \frac{1}{\kappa_w} \dot{p}_w + \nabla \cdot \boldsymbol{v} + \nabla \cdot \boldsymbol{v}_d = 0 & \text{in } \Omega_t \end{cases}$$

This system is completed with the appropriate initial and boundary conditions. $\boldsymbol{\sigma}$ stands for the Cauchy total stress, $\boldsymbol{b}$ are the external volumetric loads, $\boldsymbol{v}$ is the solid skeleton velocity and $\boldsymbol{v}_d$ is the Darcy's velocity.

The system of equations is non-linear geometrically since balance equations are imposed in the new (unknown) configuration. The proposed approach slightly differs in the treatment of some terms with respect to (Borja and Alarcón, 1995; Larsson and Larsson, 2002).

In the present implementation both equations are solved in a monolithic approach and an implicit time-marching shceme is employed. The space is discretized with linear triangles and the same shape functions are used both for displacements and water pressure. This type of elements may produce spurious oscillations in the pore pressure field in nearly undrained conditions as a result of failure to satisfy the *inf-sup* conditions. In order to alleviate these oscillations, a Pressure Laplacian stabilization term is added to the mixture mass balance equation (Presig and Prévost, 2011). This way, the weak form of the problem is slightly modified so that improved numerical stability is achieved without compromising consistency.

2.3. Constitutive relations

In this work, a hyperelastic-based finite strains elasto-plastic constitutive response is assumed for the solid skeleton. The elastic model is defined by the Houlsby (1985) hyperelastic model; then, the effective volumetric and deviatoric Kirchhoff stresses - $\boldsymbol{\tau}' = J\boldsymbol{\sigma}' = \boldsymbol{\tau}_d + \theta' \boldsymbol{I}$ where J is the Jacobian (a measure of the volume change) and $\boldsymbol{\sigma}'$ is the effective Cauchy stress tensor - are obtained as:

$$\begin{cases} \theta' = -p_r e^{\frac{-\varepsilon_v^e}{\kappa^*}} (1 + \alpha \|\boldsymbol{\varepsilon}_d^e\|^2) \\ \boldsymbol{\tau}_d = 2 \left(G_0 + \alpha\, p_r e^{\frac{-\varepsilon_v^e}{\kappa^*}} \right) \boldsymbol{\varepsilon}_d^e \end{cases}$$

where $\boldsymbol{\varepsilon}^e$ is the elastic Hencky Strain, $\kappa^* = \frac{\kappa}{1+e_0}$, κ is the swelling slope, G_0 is the constant part of the shear modulus, p_r is a reference pressure and $\alpha \geq 0$ is a parameter that controls the coupling of the volumetric and deviatoric response and the Poisson's ratio.

The problem is completed with the Modified Cam Clay yield surface and hardening law (Borja et al, 2002):

$$\psi(\boldsymbol{\tau}') = \left(\frac{\sqrt{3} J_2}{M(\theta_L)} \right)^2 + \theta'(\theta' - p_c) \leq 0$$

$$p_c = -p_{c0} e^{\frac{-\varepsilon_v^p}{\lambda^* - \kappa^*}}$$

where J_2 is the second stress invariant, θ_L is the Lode's angle, p_c is the preconsolidation pressure, ε_v^p is the Hencky volumetric plastic strain, $\lambda^* = \frac{\lambda}{1+e_0}$ and λ is the slope of the normal compression line.

The integration of stresses is performed with an explicit integration scheme with adaptive sub-stepping and a correction for the yield surface drift is applied (Monforte et al, 2014).

2.4. Contact Constraints

The interaction between multiple bodies produces a set of normal and tangential forces in the interface. Mathematically, contact conditions are expressed as a set of geometrical restrictions to the solution. Indeed, one of the contacting bodies –the structure- is assumed rigid; this hypothesis is valid when the ratio between the soil and structure Young's moduli is large (Sheng et al, 2005).

In this work, the contact constraints are imposed to the solution with the penalty method; this way, the restrictions are only approximately fulfilled.

The tangential part of the contact is idealized with an elasto-plastic analogy, where the so-called stick conditions –no tangential relative displacement between the bodies- is modelled as the elastic loading part and the slip conditions –which is characterized by the relative tangential movement- is represented by plastic flow.

A Coulomb law is used as the yield surface of the tangential part of the contact:

$$f(\sigma_n', \tau) = \tau - \mu \sigma_n' \leq 0$$

where σ_n' is the normal effective stress acting at the interface, τ is the interface tangential stress, $\mu = \tan(\delta)$ and δ is the interface friction angle.

3. NUMERICAL ANALYSIS

In this section, first a benchmark example –the oedometer test- is presented to assess the implementation; then, the constitutive model is exemplified with a constant volume shear test. Finally, a parametric analysis of the CPT is presented.

3.1. Oedometer test

The first example corresponds to an oedometer test in a weightless soil. For the sake of simplicity, in this example the soil is assumed to obey a linear hyperelastic behaviour.

Small strains analytical solutions states that the key constitutive parameter that controls the pore pressure dissipation is the coefficient of consolidation, $c_v = \frac{M k}{\gamma_w}$, where M is the constrained modulus. In order to evaluate large strains effects, the same problem has been computed with two sets of parameters maintaining constant the coefficient of consolidation, $c_v = 2.7 \cdot 10^{-3} \frac{m^2}{s}$, and the Poisson's ratio, $\nu = 0.3$. Two Young's modulus have been used: $E = 2 \cdot 10^2$ kPa and $E = 2 \cdot 10^5$ kPa.

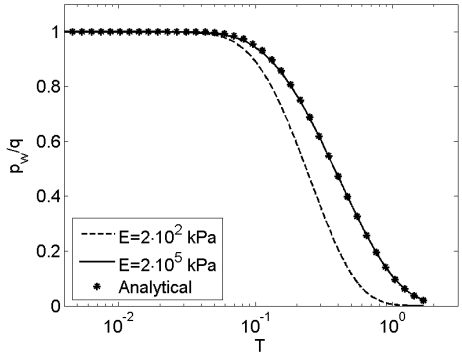

Figure 1: Oedometer test. Dissipation curves for two sets of parameters.

Figure 1 shows the variation of the water pressure at the bottom of the sample as a function of the time factor for the two sets of parameters. In the larger Young's modulus case, both displacements and deformations are small and the solution agrees well with the small strains analytical solution. The other case is different due to the severe geometric non-linearity: as consolidation takes place, the height of the domain decreases; thus, the draining path length reduces, see Figure 2.

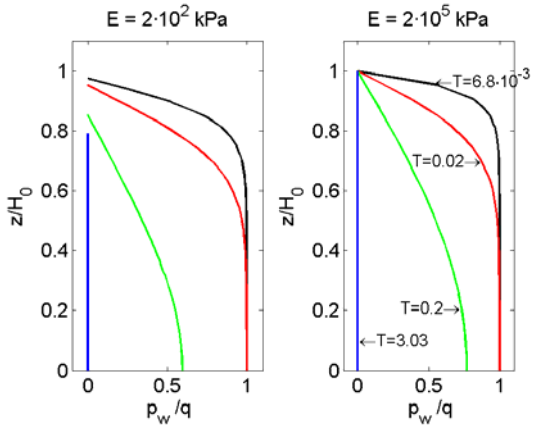

Figure 2: Oedometer test. Isochrones of the water pressure for two sets of parameters.

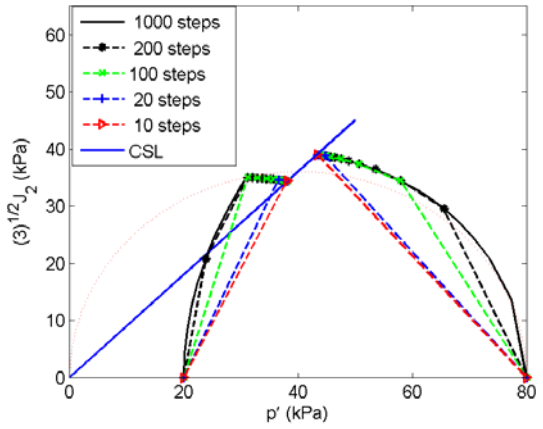

Figure 3: Constant volume simple shear test. Effective stress trajectory in the p-$3^{0.5}J_2$ plane for *OCR* =1 and 4 for different temporal discretizations.

3.2. Constant volume simple shear test

The current example consists on a constant volume simple shear test and serves to validate the numerical implementation of the constitutive model. The same constitutive parameters than a reference solution are used (Rouainia and Muir Wood, 2000).

This example consists on the evaluation at one Gauss point of a displacement-driven problem. The displacement field is parameterized by a pseudo-time variable, t, and is written as: $\mathbf{u}(x, y, z, t) = (yt, 0, 0)$, for $0 \leq t \leq 1$.

Two different analyses have been performed with different overconsolidation ratios (*OCR*). In both cases the preconsolidation pressure is equal to 80 kPa and in one case the analysis starts at normally consolidated conditions whereas in the other the OCR is equal to 4. In both cases the analysis begins at hydrostatic stress.

Figure 3 shows the effective stress trajectories; both tests tend to the critical state line. As it can be seen in the overcosolidated test, there exists a change in mean stress at constant volume in elastic regime due to the coupling in the non-linear hyperelastic model. Then, the stress state tends to the critical state line in elasto-plastic regime. Note than these effective stress trajectories are the same to an undrained triaxial test.

The obtained results are in good agreement with those reported by the reference solution using an implicit stress integration technique. In addition, Figure 3 also shows the stress trajectories computed with different time discretization: the problem has been computed with a different number of steps, ranging from 10 to 1000 steps. In both cases, the solution computed with a small number of steps converges towards that obtained with a larger resolution and minimal discrepancies between them exists; this is due to the use of an adaptive substepping algorithm.

3.3. Cone Penetration Test

The last numerical analysis consists on the penetration of a CPT in a Modified Cam Clay soil. Several simulations are presented with different permeabilities and interface friction angles and attention is paid at variations of the net cone resistance, the friction sleeve resistance and the water pressure at three positions: u_1 position (at the midface of the cone), u_2 position (at the apex between the cone and the shaft) and u_3 position (above the friction sleeve, at 7.5 cone radii above the apex). Four different permeabilities have been considered, $K = 3.3 \cdot 10^{-6}$, $5 \cdot 10^{-7}$, 10^{-7}, 10^{-9}, m/s and two different interface friction angles, $\delta = 0°$ and $\delta = 14°$. The eight combinations have been considered.

The basic constitutive parameters are listed in Table 2; the selected values try to mimic the example reported by Sheng et al (2014), where a parametric analysis of the effect of the penetration velocity for smooth CPT is presented. In this work, the self weight of the soil has been omitted and the initial effective stress and water pressure have been chosen similar those encountered at the final penetration depth of the reference solution.

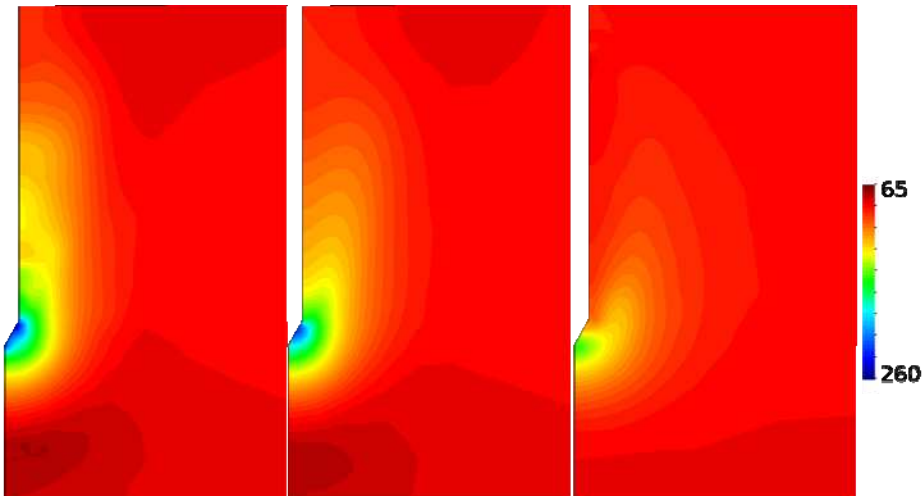

Figure 4: Cone penetration test. Water pressure (kPa) profiles at the final penetration depth for different permeabilities: K = 10^{-7} m/s (left), K = $5 \cdot 10^{-7}$ m/s (center), K = $3.3 \cdot 10^{-6}$ m/s (right) for smooth interface.

Table 1: Cone penetration test. Constitutive parameters adopted for the Modified Cam Clay model

κ^*	λ^*	α	G_0(kPa)	p_0(kPa)
0.016	0.1	23.5	400	10
p_{c0}(kPa)	M	σ'_{v0}(kPa)	σ'_{h0}(kPa)	p_{w0}(kPa)
70	1	57.5	28.9	80

In the beginning of the computation the cone is assumed in a wished-in-place situation at a depth of 3 cone radii. Then cone is pushed at the standard velocity ($v_c = 0.02$ m/s). The domain is 28 times the cone radius in with and 56 times in depth. The bottom boundary of the soil domain is assumed to be fully drained (fixed water pressure). A constant vertical stress is applied at the top boundary. The radial displacement is fixed at the left and right boundaries whereas null displacement in all directions is imposed at the bottom boundary.

Figure 4 shows the water pressure profiles at the final penetration depth for the smooth case. When low permeabilities are considered, the maximum of the water pressure is found below the apex between the tip and the shaft and decreases in all directions. In addition, large excess water pressures are found along the shaft of the structure. In the three cases with the lowest permeability, a negative excess water pressure occurs below the cone tip and the magnitude is larger with lower permeabilities.

The penetration in the lowest permeability case takes place in almost undrained conditions: results reveal that the volumetric deformation is small, less than 0.1% in the entire domain. In contrast, in the other scenarios with grater permeabilities largest volume deformations are found whereas lower excess pore water pressure are encountered with respect to the previous case, confirming that penetration takes place in partially drained conditions. These observations are common for both interface friction angles.

Figure 5 shows the evolution of the net cone resistance, the water pressure at the measurement positions and the sleeve friction resistance as a function of penetration depth. In all the cases a clear stationary state of the net cone resistance and water pressure at the u_1 and u_2 position is achieved after a penetration of approximately of 7 radii. At the first 6 radii of penetration the sleeve friction resistance increases rapidly; at this depth all the friction sleeve is in contact with the soil. Then, the friction sleeve resistance varies until a stationary value is found. In some of cases, it is unclear if the water pressure at the u_3 position and the sleeve friction reach a stationary value.

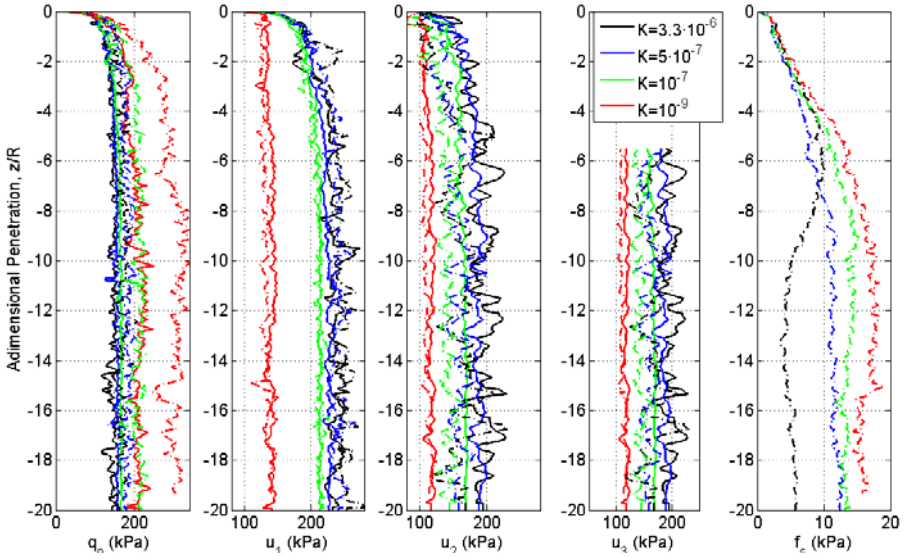

Figure 5: CPT. Net cone resistance (q_n), water pressure at the three measurement positions and friction sleeve resistance in terms of the penetration depth. Smooth cases (continuous lines) and rough cases (discontinuous lines).

The reported curves present some oscillations that are more pronounced when a rough contact is employed and in the lowest permeability case. These oscillations are interpreted as the mesh-dependence of the solution and error introduced in the transfer of variables between different finite element meshes. For the smooth case, the obtained results compare well with those reported by the reference solution (Sheng et al, 2014) that uses a different implementation of the Modified Cam Clay.

Figure 6 shows the mean value at the last 10 penetration radii of the relevant CPT reactions in terms of the interface friction angle and the dimensionless penetration velocity, v_c/k. The net cone resistance increases with the permeability; the lowest cone resistance corresponds to the undrained case. When the interface between the clay and the soil is assumed rough, the cone resistance increases at a steeper rate as the permeability increases.

The smallest friction sleeve resistance is found in the undrained analysis and it increases with larger permeabilities. On the other hand, the friction ratio, $f_r = \frac{f_s}{q_n}$, varies between 2.9% and 6.4%; the minimum and maximum are observed in the two lowest permeability scenarios.

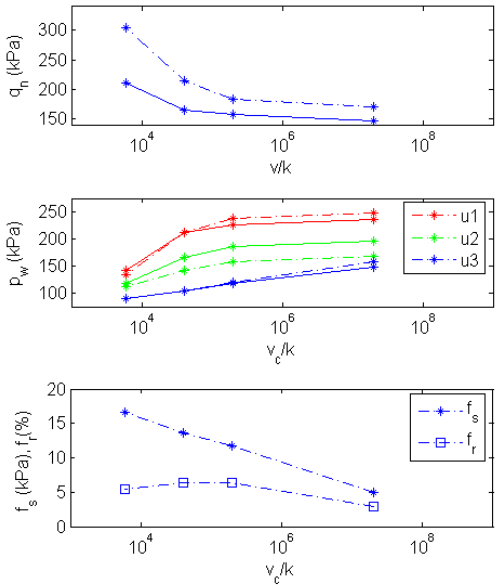

Figure 6: CPT. Steady state net cone resistance, water pressure and friction resistance f_s and ratio f_r in terms of the dimensionless velocity. Smooth (continuous) and rough (discontinuous).

The water pressure at the three locations decreases as permeability increases. The largest water pressure is found in the u_1 position whereas the lowest one is in the u_3 position. In addition, in the simulations that assume a rough

interface, the water pressure at the u_1 position is slightly larger than the one encountered with a smooth interface; on the other hand, the water pressure in the u_2 position is lower considering a rough interface.

4. CONCLUSIONS

In this work, a numerical framework for the analysis of saturated porous media undergoing large deformations has been presented. By means of the analysis of the oedometer test is has been shown that the obtained results are accurate; indeed, using a large deformation theory may reflect results that are artificially excluded by the linear theory.

Preliminary results of a parametric analysis of the Cone Penetration Test in a Modified Cam Clay soil have been reported. The effect of the interface friction angle and the permeability of the soil on the measured reactions has been assessed.

The developed numerical scheme appears to be a promising tool for the simulation of penetration problems in geotechnics.

ACKNOWLEDGEMENTS

The author would like to thank his thesis supervisors, Prof Antonio Gens, Dr Marcos Arroyo and Dr Josep Maria Carbonell, for their guidance during this work.

The financial support of the Sociedad Española de Mecánica de Suelos to cover the expenses of the trip is acknowledged.

The support of the Ministry of Education of Spain through research grant BIA2011-27217 is gratefully appreciated.

REFERENCES

Borja, R.I. & Alarcón, E (1995) “A mathematical framework for finite strains elastoplastic consolidation. Part I”, Comput. Methods in App. Mech. and Eng., 122(1-2):145-171.

Houlsby, G.T. (1985) ”The use of variable shear modulus in elasto-plastic models for clays”, Computers and Geotechnics, 1(1):3-13.

Larsson, J & Larsson, R (2002) ”Non-linear analysis of nearly saturated porous media: theorical and numerical formulation”, Comput. Methods in App. Mech. and Eng., 191(1):3885-3907.

Monforte, L., Arroyo, M., Gens, A. & Carbonell, J.M. (2014) ”Explicit finite deformation stress integration of the elasto-plastic constitutive equations”, Computers Methods and Recent Advances in Geomechanics – Proceedings of the 14th Int. Conf. of IACMAG, 267-272.

Oñate, E., Idelsohn, S.R., del Pin, F. & Aubry, R. (2004) ”The Particle Finite Element Method. An overview”, International Journal of Computational Methods, 1(2):267-304.

Preisig, M. & Prévost, J.H. (2011) “Stabilization procedures in coupled poromechanics problems: A critical assessment”, Int. J. Numer. Anal. Meth. Geomech., 35:1207-1225.

Rounainia, M. & Muir Wood, D. (2000) “An implicit constitutive algorithm for finite strain cam clay elasto-plastic model”, Mechanics of Cohesive-frictional materials, 5(6):469-489.

Sheng, D., Eigenbrod, K.D. & Wriggers, P. (2005) “Finite element analysis of pile installation using large-slip frictional contact”, Computers and Geotechnics, 32(1):17-26.

Sheng, D., Kelly, R., Pineda, J. & Lachlan, B. (2014), “Numerical study of rate effects in cone penetration test”, 3rd International symposium on Cone Penetration Testing, 419-428.

Tsubakihara, Y. & Kishida, H (1993) “Frictional behaviour between normally consolidate clay and steel by two direct shear type apparatuses”, Soils and Foundations, 33(2):1-13.

Yi, J.T., Goh, S.H., Lee, F.H. and Randolph, M.F. (2012) “A numerical study of cone penetration in fine-grained soils allowing for consolidation effects”, Geotechnique, 62(8):707-719.